

The HYPERMAQ dataset-: bio-optical properties of moderately to extremely turbid waters

Héloïse Lavigne¹, Ana Dogliotti², David Doxaran³, Fang Shen⁴, Alexandre Castagna⁵, Matthew Beck¹, Quinten Vanhellemont¹, Xuerong Sun⁴, Juan Ignacio Gossn^{2,7}, ~~Renosh Pannimpullath~~³ Pannimpullath Remanan Renosh³, Koen Sabbe⁵, Dieter Vansteenwegen⁶, Kevin Ruddick¹

¹ Royal Belgian Institute of Natural Sciences, Brussels, Belgium

² Instituto de Astronomía y Física del Espacio (IAFE), CONICET-Universidad de Buenos Aires, Buenos Aires, Argentina

³ Laboratoire d'Océanographie de Villefranche, UMR7093 Sorbonne Université /CNRS, Villefranche-sur-Mer, France

⁴ State Key Laboratory of Estuarine and Coastal Research (SKLEC), East China Normal University, Shanghai, China

⁵ Laboratory of Protistology and Aquatic Ecology, Ghent University, Ghent, Belgium

⁶ ~~Flanders~~ Flanders Marine Institute (VLIZ), Ostend, Belgium

⁷ ~~European~~ European Organisation for the Exploitation of Meteorological Satellites (EUMETSAT), Darmstadt, Germany.

Correspondence to: Héloïse Lavigne (hlavigne@naturalsciences.be)

Abstract. Because of the large diversity of case 2 waters ranging from extremely absorbing to extremely scattering waters and the complexity of light transfer due to external terrestrial inputs, retrieving main biogeochemical parameters such as chlorophyll-a or suspended particulate matter concentration in these waters is still challenging. By providing optical and biogeochemical parameters for 180 sampling stations with turbidity and chlorophyll-a concentration ranging from 1 to 700 FNU and from 0.9 to 180 mg m⁻³ respectively, the HYPERMAQ dataset will contribute to a better description of marine optics in optically complex water bodies and can help the scientific community to develop algorithms. The HYPERMAQ dataset provides biogeochemical parameters (i.e. turbidity, pigment and chlorophyll-a concentration, suspended particulate matter), apparent optical properties (i.e. water reflectance from above water measurements) and inherent optical properties (i.e. absorption and attenuation coefficients) from six different study areas. These study areas include large estuaries (i.e. the Rio de la Plata in Argentina, the Yangtze Estuary in China and the Gironde Estuary in France), inland (i.e. the Spuikom in Belgium and Chascomús lake in Argentina) and coastal waters (Belgium). The dataset is available from Lavigne et al (2022), <https://doi.pangaea.de/10.1594/PANGAEA.944313>.

a mis en forme : Police :Gras

1 Introduction

In marine optics, certain water properties such as the concentration of chlorophyll-a ([Chl-a] hereafter) or suspended particulate matter (SPM hereafter) are inferred from water leaving reflectance allowing a powerful satellite based monitoring. However, although algorithms are well matured in clear case 1 waters (Morel and Prieur, 1975; Morel and Maritorena, 2001), it is not the case in optically complex case 2 waters where apparent optical properties

39 (AOPs) and inherent optical properties (IOPs) are influenced not only by [Chl-a] but also by terrestrial optically-
40 active substances such as suspended sediments and colored dissolved organic matter (CDOM) that do not covary
41 with [Chl-a]. Given the complexity of light transfer in these waters and the large diversity of case 2 waters, algo-
42 rithm definition is much more challenging (Odermatt et al., 2012) and requires datasets covering the extreme
43 variability of case 2 water conditions. Hence, any additional data obtained in optically complex waters are valuable
44 to the scientific community as they will help to better understand marine optics in such waters and to design ocean
45 color algorithms.

46 The present dataset (Lavigne et al., 2022; <https://doi.pangaea.de/10.1594/PANGAEA.944313>) has been collected
47 as part of the HYPERMAQ project. During this project, different types of optically complex waters with turbidity
48 ranging from moderate to extreme (1 to 700 FNU) and [Chl-a] ranging from low to very high (0.9 to 180 mg m⁻³)
49 have been sampled in various locations around the world. Their main optical and biogeochemical parameters
50 are shared in this dataset, including measurements of water-leaving reflectance, turbidity, non-water light absorp-
51 tion and attenuation coefficients as well as SPM, [Chl-a] and other pigment composition. In the next sections,
52 study areas, sampling methodology and final HYPERMAQ datasets are described.

a mis en forme : Police :Non Italique

53 2 Sites

54 Different sites, generally characterized as optically complex case 2 waters with a turbidity and [Chl-a] ranging
55 from moderate to extremely high, have been sampled in coastal and inland waters in Belgium, France, Argentina
56 and China (Figure 1). Contrary to case-1 waters, optical properties of case-2 waters are impacted by terrestrial
57 inputs of sediments and CDOM with concentrations ranging from low to extreme values. Hence, in these waters,
58 the retrieval of water properties from bio-optical algorithms is extremely complex. As case-2 waters are generally
59 highly connected to land-ocean interaction and human activities (estuaries, coastal and inland waters), it becomes
60 critical to collect enough in situ data to help for the development of specific algorithms. Given the large diversity
61 of case-2 waters, Hieronymi et al. (2016) defined four main groups: case-2 scattering (C2S), case-2 extremely
62 scattering (C2SX), case-2 absorbing (C2A) and case-2 extremely absorbing (C2AX), suggesting that specific ef-
63 forts in algorithm development should be given to each group. For instance, Hieronymi et al. (2017) proposed a
64 multi-neural networks algorithm for case-2 waters atmospheric correction, but the algorithm was mostly trained
65 and validated with synthetic datasets. In this context, the HYPERMAQ dataset provides bio-optical data from C2S
66 and C2SX waters by sampling a very large diversity of waters affected by additional sediments inputs (see sample
67 sites on Figure 1). Sample sites allow obtaining a large range in SPM and turbidity (1 to 700 FNU) by sampling
68 Belgian coastal waters which are extremely turbid locally close to the coast and less turbid further offshore. In
69 addition, three estuaries known to be extremely turbid have been sampled (the Gironde (France), the Yangtze
70 (China) and the Rio de la Plata (Argentina) estuaries). Since they are affected by tides, a gradient of turbidity could
71 be sampled along the day with diverse influences of oceanic waters. These three estuaries, located on different
72 continents, carry suspended particles with their own mineral properties, enriching then the database. Finally, two
73 terrestrial lagoons were sampled. One with low to moderate concentrations in suspended sediments (Spuikom in
74 Belgium) and one with extreme concentrations of both algae and non-algal suspended particles (Chascomùs in

75 [Argentina\). This large diversity of sampled sites should then help to improve our knowledge of case-2 moderately](#)
76 [to extremely scattering waters. A detailed description of each site is provided below.](#)

77

a mis en forme : Couleur de police : Rouge

78 2.1 Belgian coastal waters

79 The Belgian coastal waters (latitudes:51.27° to 51.59°N; longitudes: 2.50° to 3.15°E) have been sampled in April
80 2018 and July 2018 from the RV Simon Stevin (Table 1). Belgian coastal waters are dominated by Atlantic waters
81 which enter from the English Channel (Lacroix et al., 2004) and experience very strong along shore tidal currents
82 which cause sediment resuspension leading to high turbidity. SPM concentrations range from less than 1 g m⁻³ in
83 offshore and deeper waters to more than 100 g m⁻³ in very shallow waters. Phytoplankton blooms, characterized
84 by high [Chl-a] concentration (more than 10 mg m⁻³), develop in spring from March to May. During summer, the
85 biomass remains rather high (5 to 10 mg m⁻³) compared to winter when phytoplankton growth is mostly limited
86 by light (Lancelot et al., 2005). The blooming season is mostly dominated by two taxa: diatoms in early spring and
87 summer and *Phaeocystis globosa* in April-May (Muylaert et al., 2006).

88 2.2 Spuikom lagoon

89 The Spuikom lagoon (latitude: 51.23°N, longitude: 2.95°E) is an artificial basin that is connected to Ostend harbor
90 (Belgium) by a lock system. The Spuikom has a surface area of 0.82 km² and an average depth of 1.5 m. In the
91 past, it has been used as a flushing basin to flush sediments from the harbor channel. Today it is used for leisure
92 and commercial activities like sailing and shellfish farming. The Spuikom can experience events of phytoplankton
93 blooms, of high turbidity (when strong winds cause the resuspension of bottom sediments), and of clear waters,
94 which allow the development of microphytobenthic biofilms and macroalgae in the bottom (Castagna et al., 2022).
95 The system was sampled during the growth season of 2018 (April and July, Table 1). Measurements were
96 performed from inflatable boats provided by Ghent University and VLIZ (Zeekat).

97 2.3 Gironde Estuary

98 The Gironde Estuary, southwest France, is a good example of sediment-dominated case 2 waters influenced by
99 river inputs. The Gironde Estuary has been sampled between 17-20 September 2018 in two locations: Pauillac
100 (latitude: 45.1975°N, longitude: -0.7422°E) close to the maximum turbidity zone and Le Verdon (latitude:
101 45.5438°N, longitude: -1.042°E) close to the river mouth. In the Gironde Estuary, the origin of the particles is
102 twofold: inputs from rivers Garonne and Dordogne ~~and erosion~~ and erosion of recently settled sediments by tidal
103 currents (Castaing and Allen, 1981). The suspended matter is a mixture of organic and mineral composites, where
104 the organic fraction represents less than 2% of the total material (Doxaran et al. 2002). The mineral fraction is
105 composed of micas (63%) and quartz (25%), while clay phases contain four minerals: montmorillonite (30%),
106 illite and interstratified minerals (40%), kaolinite (15%), chlorite and interstratified minerals (15%). [Chl-a] and
107 CDOM concentrations are low, with [Chl-a] ranging from 1 to 3 mg m⁻³ (Irigoiien & Castel, 1997), and dissolved
108 organic carbon (DOC) ranging from 1 to 7 mgC L⁻¹ (Abril et al., 1999; Castaing and Allen, 1981). The Gironde
109 Estuary has well-developed turbidity maximum zones, with both tidal asymmetry and density residual circulation

110 involved in their formation (Castaing and Allen, 1981). It is characterized by SPM concentrations ranging from 10
111 to 1000 g m⁻³ within surface waters (Doxaran et al. 2009a).

a mis en forme : Non Exposant/ Indice

112 2.4 Chascomús lake

113 Chascomús lake, located in the Pampa Plain in the Buenos Aires Province in Argentina (latitude: -35.5828°N,
114 longitude: -58.0202°E), with a surface area of ~ 30 km², is a highly turbid, shallow lagoon (average depth of ~ 1.9
115 m), permanently mixed due to intense and persistent winds (Torremorell et al., 2007). Total suspended matter
116 varies widely from 66.3 to 614 g m⁻³ with a mean value of 227.3 ± 133.7 g m⁻³ (Diovisalvi et al. 2014) and on
117 average the inorganic content represented ~65%. Nephelometric turbidity also widely ranged from 76.46 to 509.74
118 NTU, with a mean value of 209.18 ± 112.76 NTU. Turbidity was highly correlated to SPM while no significant
119 correlation with [Chl-a] was found (Pérez et al. 2011). Total [Chl-a] concentration ranged from 50.6 to 856.3 mg
120 m⁻³ (mean = 328.5 ± 173.4 mg m⁻³) during the 2005-2009 sampled period (Diovisalvi et al. 2014). The lake is
121 characterized by high primary production (Torremorell et al., 2009) and a rich and diverse phytoplankton commu-
122 nity, mostly composed of cyanobacteria. In terms of biovolume, cyanobacteria contribute 50% to total phytoplank-
123 ton biovolume and 75% to total C in the water column (Diovisalvi et al. 2010). Despite the high CDOM absorption
124 (a_{CDOM} , mean $a_{CDOM}(440) = 4.65 \pm 0.91 \text{ m}^{-1}$), absorption by particulate fraction (a_p) has a prominent role in light
125 absorption, for which both phytoplankton pigments (a_{phy}) and non-pigmented particles (a_{NAP}) contribute similarly
126 to total particulate absorption (Pérez et al. 2011). Both SPM (especially the inorganic part) and [Chl-a] (less pro-
127 nounced) show seasonal variation with increasing values in spring and summer (Mid-September to Mid-March),
128 while the dissolved fraction did not show a significant seasonal difference (Pérez et al. 2011). The HYPERMAQ
129 field campaign in Chascomús lake took place on 9-10 April 2018. Radiometric, in-water measurements as well as
130 samples were collected at the end of a 164 m long pier.

a mis en forme : Police :Non Italique

131 2.5 Río de la Plata

132 The Río de la Plata is a large and shallow funnel shaped estuary with high values SPM, ranging from 100 to 300
133 g m⁻³ (Framiñan and Brown, 1996) and reaching 940 g m⁻³ in the maximum turbidity zone (Dogliotti et al. 2014).
134 Turbidity values widely vary between 2 and 680 FNU (Dogliotti et al. 2016). SPM, turbidity and [Chl-a] spatial
135 distribution and temporal variability is highly variable. In the upper estuary, a freshwater with tidal regime area,
136 turbidity increases from January to April/May (with higher values along the southern Argentinian coast ~~of~~ com-
137 pared to the northern Uruguayan coast), and decreases from June to September (Dogliotti et al. 2016). In turn [Chl-
138 a] also show high spatial variability, in the upper estuary higher values are generally found in the northern part
139 (Uruguay) compared to the southern part (Argentina). In particular, high [Chl-a] have been recorded during spring-
140 summer months related to cyanobacteria blooms both along the Uruguay (Aubriot et al. 2020) and Argentine
141 (Dogliotti et al. 2021) coasts, when [Chl-a] values as high as 13.6 and 153 mg m⁻³ have been recorded, respectively.
142 Measurements in the Río de la Plata were performed from a fixed 500 m long pontoon at the Palermo Pescadores
143 Club in Buenos Aires (latitude: -34.5609°N, longitude: -58.3988°E) on 4 and 5 April 2018.

144 2.6 Yangtze Estuary

145 The Yangtze Estuary is located on the east coast of China and close to East China Sea (Figure 1). Influenced by
146 the Yangtze River, the largest river in China and the third largest in the world [due to its enormous runoff](#), which
147 discharges an annual average of 9×10^{11} m³ of freshwater and 4×10^8 tons of sediment into the estuary [from 1950s](#)
148 [to 2000](#) (Chen et al., 2003), the Yangtze Estuary is an extremely turbid area (Shen et al., 2010a). Taking 2009 as
149 example, the annually averaged of SPM in surface waters varied from 58 g m⁻³ at the upstream limit of the estuary
150 to about 600 g m⁻³ at the mouth area, and fell again to 57 g m⁻³ at the seaward limit of fresh water diffusion (Li et
151 al., 2012). Due to the different river discharges, the SPM of the Yangtze Estuary exhibits seasonal variations (Shen
152 et al., 2013), with SPM in the upper estuary (lower estuary) during flood season significantly higher (lower) than
153 that during the dry season. Over the past 37 years, SPM in [the](#) Yangtze Estuary demonstrated an overall declining
154 pattern (Luo et al., 2022), with SPM in the inner estuary responding most promptly (40.3% reduction) after the
155 operation of Three Gorges Dam. [Chl-a] also shows seasonal variations in [the](#) Yangtze Estuary, ranging from 0.03
156 to 3.10 mg m⁻³ and from 0.88 to 31.5 mg m⁻³ during spring and summer seasons of 2008, respectively (Shen et al.,
157 2010b). In addition, the Yangtze Estuary is an area with frequent outbreaks of algal blooms, with diatoms being
158 the most frequently reported group (Shen et al., 2019; Zhu et al., 2019).

159 Two Hydrological Stations in Chongming Island, Shanghai, China, namely Chongxi (longitude:121.193°E,—, _lat-
160 itude:31.759°N) and Baozhen (longitude:121.609°E,—, _latitude:31.520°N) have been sampled from 30 May to 8
161 June in 2018 (Table 1).

162

163 3. Data collection

164 The dataset contains measurements of the turbidity and, if available, concomitant SPM, absorption and attenuation
165 coefficients, [Chl-a] and reflectance measurements are also included (Lavigne et al., 2002; <https://doi.pangaea.de/10.1594/PANGAEA.944313>). An overview of the dataset, with the number of observations after quality
166 control for each site and parameter, is provided in Table 2. The measurement methodology for each parameter is
167 described below.

169 3.1 Water-leaving reflectance

170 Above-water reflectance was determined using three TriOS/RAMSES hyperspectral spectroradiometers, two spec-
171 troradiometers measure radiance and one irradiance. The same TriOS instruments from RBINS institute were used
172 for all campaigns except the ones which occurred in Argentina where only instruments from IAFE institute were
173 available. The spectrometers measure in the 350-950 nm range with a sampling interval of 3.3 nm and effective
174 spectral resolution of 10 nm. The instruments were mounted on a frame and placed in the bow of the vessels
175 (Belgian coastal zone and Spuikom) or fixed to a rail when measurements were made from pontoons (Gironde,
176 Chascomús and Rio de la Plata). Zenith angles of the sea- and sky-viewing radiance sensors were set to 40°. Prior
177 to each measurement, the azimuth angle of the sensors was adjusted to obtain a relative azimuth angle with respect
178 to the sun of 90°, either left or right to get the best unobstructed view of the water and minimize structure pertur-
179 bation when measuring from pontoons. Simultaneous upwelling water radiance (L_u), downwelling sky radiance

180 (L_{sky}) and downwelling irradiance (E_d) were collected every 10 s for 10 min. Data was acquired using MSDA-XE
181 software and radiometrically calibrated using the latest calibration update from annual laboratory calibration. Wa-
182 ter reflectance (ρ_w) was calculated following

$$183 \quad \rho_w(\lambda) = \frac{L_u(\lambda) - \rho_{sky}L_{sky}(\lambda)}{E_d(\lambda)}\pi$$

184 Where ρ_{sky} is the air-sea interface reflection coefficient which is calculated based, when available, on wind speed
185 as in Ruddick et al. (2006) or set to a fixed value of 0.0256 when measured in estuaries from fixed pontoon con-
186 sidering that surface waves are fetch-limited and not related to wind speed. The data processing, including quality
187 control, are described in Ruddick et al. (2006).

188 3.2 Turbidity

189 Turbidity was measured with two handheld HACH 2100P/Q ISO turbidimeters from RBINS and IAFE institutions.
190 In the HYPERMAQ dataset, turbidity data measured with the instrument from IAFE were provided by default as
191 they cover the most of the campaigns. However, when turbidity data from IAFE instrument were not available
192 (Belgian coastal waters, April 2018 and Spuikom April 2018), the values obtained with the instrument of the
193 RBINS were used. Figure 2 shows the good consistency of both instruments ($r^2=0.99$). Water samples were col-
194 lected from the surface with a bucket or from subsurface with a NISKIN bottle for measurements in coastal waters.
195 A 10 mL vial was filled and turbidity was determined in Formazin Nephelometric Unit (FNU) with the ratio of
196 light scattered at 90° compared to the transmitted light at 860 nm. Turbidity was recorded in triplicates and the
197 median value was used. Turbidimeters were controlled with standards STABCAL Stabilized Formazin Turbidity
198 of 0.1, 20, 100 and 800 FNU before and after each campaign.

199 In water turbidity was also measured with an OBS501 (OBS hereafter) using a CR200 data logger. Turbidity
200 measurements are derived from back-scattering with a field-of-view ranging from 125 to 170 degree and 90-degree
201 side-scattering of a signal emitted at 850 nm and data are provided in Formazin Backscatter Unit (FBU) and in
202 Formazin Nephelometric Unit (FNU), respectively. When deployed from a pier, OBS was continuously recording
203 data at subsurface throughout the whole day and values corresponding to specific stations were extracted from the
204 time-series in a time-window of 10 minutes centered on the timing of the radiometric measurement and water
205 sampling. When deployed from a boat, the OBS was maintained at subsurface (1 m depth) for at least 5 minutes.
206 Then, from a visual check, leading and trailing data of each time-series were removed and the central values were
207 averaged to obtain a final value.

208 3.4.3 *In situ* absorption, beam attenuation and scattering coefficients

209 The underwater absorption- and attenuation-meter (AC-9, WETLabs, Inc.) used was modified to cover the visible
210 and near-infrared (NIR; ~~700 to~~ 700 to 900 nm) spectral regions. It was designed with three visible (centered at 440
211 nm, 555 nm and 630 nm) and six NIR (centered at 715 nm, 730 nm, 750 nm, 767nm, 820 nm and 870 nm) spectral
212 channels, and a short pathlength (10 cm) appropriate for turbid coastal waters. At the sampling sites, the AC-9
213 sensor was either deployed within the water column using an electrical water pump (SBE, SeaBird, Inc.) or used
214 as a bench photometer passing the water samples right after collection through the tubes by gravimetry. The AC-

215 9 data recorded just below the water surface were averaged over the last minute of acquisition to obtain the mean
216 attenuation and absorption spectra for each station. Temperature and salinity corrections were applied as recom-
217 mended by the manufacturer. As in Doxaran et al. (2007), the residual scattering effects on absorption measure-
218 ments were corrected by applying the “proportional” method using 870 nm as the reference wavelength. The scat-
219 tering coefficient was calculated as the difference between the measured beam attenuation coefficient, c_{nw} , cor-
220 rected for temperature and salinity effects, and the absorption coefficient, a_{nw} , corrected for temperature, salinity
221 and scattering effects. Those attenuation and absorption coefficients were referenced to pure water (non-water,
222 subscript “nw”), so that the scattering coefficient obtained by difference corresponds to the scattering coefficient
223 of marine particulates, b_p in m^{-1} . Small bubbles can contribute to the measured attenuation and scattering, but in
224 turbid systems particles dominate the signal. One of the main issues encountered when sampling highly turbid
225 waters was the saturation of the measured absorption and/or attenuation coefficients, which sometimes occurred
226 at short visible wavelengths and even in near-infrared bands in the case of extremely turbid waters. This saturation
227 was easily detected and the corresponding spectra were systematically removed from the dataset.

228 When possible, after AC-9 data measurements, the water sample collected was directly filtered through disc filters
229 (pore size 0.2 μm , Whatman). As in Doxaran et al. (2009b), the tube was rinsed twice with Milli-Q water and once
230 with the filtrate, and then filled with the filtrate. The absorption signal of the filtrate was measured, providing
231 a_{CDOM} in m^{-1} after applying corrections for temperature and salinity. The absorption coefficient of suspended
232 particles (a_p , in m^{-1}) was finally calculated by subtracting the signal from the non-water absorption coefficient.

233 3.5.4 Concentration of Suspended Particulate Matter and Suspended Inorganic Particulate Matter

234 SPM concentration was determined gravimetrically following the protocol of Tilstone et al. (2002) which is based
235 on Van der Linde (1998). Water was sampled from the surface (maximum ~~2 m~~ 2 m depth) with a NISKIN bottle
236 on board the RV Simon Stevin or with a bucket in estuarine and inland waters. A sufficient volume of water was
237 filtered on a pre-ashed GF/F filter and conserved at $-20^{\circ}C$ before analysis. The volume filtrated was determined
238 as a function of the turbidity following recommendations of Neukermans et al. (2012). Inorganic suspended par-
239 ticulate matter (SPIM) was also calculated in all campaigns except in the Yangtze river. All the SPM measurements
240 have been conducted with 3 replicates to assess variability except for the campaigns in the Yangtze Estuary where
241 only one sample has been measured per each station. Filters were dried at $75^{\circ}C$ for 24 hours and weighed in order
242 to determine the suspended matter concentration (SPM, in $g m^{-3}$). For SPIM measurements, filters were then
243 burned at $450^{\circ}C$ for 4 hours to remove the organic part, and weighed again to estimate the suspended inorganic
244 particulate concentration (SPIM, in $g m^{-3}$).

245 3.6.5 Chlorophyll-~~a and~~ and other pigment concentrations

246 ~~{Chl-a} and phytoplankton~~ Phytoplankton pigments including [Chl-a] were determined using High Performance Liq-
247 uid Chromatography (HPLC) following the protocol of Van Heukelem and Thomas (2001) in campaigns in the
248 Belgian coastal waters, the Spuikom and the Gironde. In Belgian coastal waters, measurements were provided by
249 the LifeWatchBE sampling campaigns (Mortelmans et al., 2019, Flanders Marine Institute, 2021) of VLIZ.
250 Pigment standards were acquired from the Danish Hydrographic Institute (DHI). In the Gironde, the analysis of

a mis en forme : Police :11 pt, Couleur de police : Noir

251 pigments were performed by the SAPIGH analytical platform of the “Institut de la Mer de Villefranche” (CNRS-
252 France). In the Argentinian campaigns [Chl-a] was determined spectrophotometrically using hot ethanol (60-70
253 °C) (Jespersen and Christoffersen 1987). As for turbidity and SPM, water samples have been collected from sur-
254 face water with a bucket in inland waters or subsurface waters with a NISKIN in sea water.

255 4. Results and discussions

256 4.1 SPM and turbidity results

257 In the HYPERMAQ dataset SPM ranges between 1 g m^{-3} and 474 g m^{-3} (Table 3) and turbidity measured from
258 HACH and OBS (side-scattering measurements) ranges between 0.9 and 771 FNU and between 0.2 and 632 FNU
259 respectively. A very good relationship is observed between SPM and turbidity which almost follows the 1:1 line
260 for both instruments (Figure 3). A linear model between both parameters gives very good coefficients of determi-
261 nation ($R^2 = 0.98$ for HACH and $R^2 = 0.95$ for OBS) and slopes (0.92 for HACH and 0.86 for OBS). However, we
262 can notice that for very high turbidity (> 500 FNU), turbidity values measured by HACH tends be slightly higher
263 than SPM values (Figure 3A) but not OBS turbidity values. As expected from previous results, when comparing
264 side scattering turbidity obtained from OBS and turbidity measured by HACH, a good relationship is retrieved
265 (Figure 4A) with a R^2 of 0.96 and a slope of 0.84. Despite larger variability for very high turbidity, these results
266 confirm that OBS is a good tool for continuous measurements of turbidity in turbid environments.

267 The ratio of the side scattering versus the back scattering derived from OBS measurements has a particular interest
268 as it can provide information on the size and properties of the particles, e.g higher ratio could be explained by
269 larger particles (Nechad et al., 2016). In the HYPERMAQ dataset this ratio (Figure 4B) displayed a very high
270 variability in low turbidity environments and an increasing slope for high turbidity environments (i.e. Pauillac) as
271 also observed by Nechad et al. (2016). The very high variability when turbidity is low is explained by the strong
272 impact of uncertainty on low back scattering values in the ratio calculation. In Figure 4B, it can be observed that
273 the side scattering versus back scattering ratio varies significantly between and within sampled sites. For instance,
274 this ratio is higher in the Gironde Estuary at Le Verdon than in the Spuikom lagoon. It seems also to be higher in
275 the Río de la Plata and in the Gironde at Pauillac than in the Chascomús lake, though the Río de la Plata showed
276 high variability. Finally, the median ratio of the whole dataset is 1.77 which is close to the mean value of 1.72
277 found in Nechad et al. (2016) in turbid waters.

278 4.2 Chl-a and other pigments concentrations

279 [Chl-a] are extremely variable within HYPERMAQ test sites with values ranging between 0.91 mg m^{-3} in the
280 Gironde Estuary at Le Verdon and 180.7 mg m^{-3} in the Chascomús lake, although most of the observations
281 are within the range of 3 mg m^{-3} to 10 mg m^{-3} (Table 4). In addition, very high variability is observed within Belgian
282 waters and Spuikom, with [Chl-a] values ranging by a factor 10. This variability is mainly due to the fact these
283 study areas have been sampled at two different seasons (i.e. spring and summer).

284 Phytoplankton pigments derived from HPLC analysis were available in the Gironde Estuary, in the Belgian coastal
285 waters and in the Spuikom. The relative contribution of some key pigments for phytoplankton groups identification

a mis en forme : Exposant

a mis en forme : Anglais (États-Unis)

286 (Uitz et al., 2006; Mackey et al., 1996) are represented on Figure 5. In the Gironde Estuary, at Le Verdon, signif-
287 icant concentration of fucoxanthin, peridin and chlorophyll-b are observed suggesting that diatoms, dinoflagellates
288 and chlorophytes are co-existing at similar levels. However, at Pauillac where phytoplankton biomass is higher
289 (Table 4), the high concentration ~~in~~of fucoxanthin suggests that planktonic ~~assemblage is~~assemblages were dom-
290 inated by diatoms. In Belgian waters, high value of fucoxanthin is also observed. This pattern was expected as
291 fucoxanthin characterized the two phytoplankton groups which are dominant during spring and summer in the
292 Southern North Sea: diatoms and the prymnesiophyte ~~Phaeocystis globosa~~*Phaeocystis globosa* (Lancelot et al.,
293 2005). The last one is also characterized by the presence of chlorophyll-c₃. In the Spuikom, fucoxanthin and chlo-
294 rophyll-b show high concentrations indicating an important proportion of diatoms and chlorophytes.

a mis en forme : Police :Italique

295 4.3 Absorption and attenuation coefficients

296 Very wide ranges of light absorption and attenuation coefficients were measured as representative of low to ex-
297 tremely turbid waters. As expected in CDOM- and sediment-rich waters, the spectral variations of the non-water
298 absorption coefficients were closely following an exponential function, with decreasing values from short visible
299 to near-infrared wavelengths (Figure 6A). The respective contributions of CDOM and suspended particles to light
300 absorption at 440 nm (Figure 7) were observed to vary from 20 % to 40% for CDOM and hence from 60 % to 80%
301 for suspended particles, which could be expected in productive waters strongly influenced by sediment inputs from
302 rivers and resuspension effects.

303 The spectral variations of the non-water attenuation coefficients (c_{nw} , Figure 6B) showed a smooth decrease with
304 increasing wavelengths, closely following the power-law function with varying slopes. These variations of the
305 spectral slope are expected to be representative of different particle size distributions due to the combined influ-
306 ences of wind-driven and tidal currents, and to the mixing between mineral-rich (sediments) and organic-rich
307 (phytoplankton) particles.

308 4.4 Water reflectance

309 The large diversity of water-leaving reflectance spectra is displayed in Figure 8. Maximum reflectance in each
310 spectrum varies from less than 0.02 on some spectra of the Belgian coastal waters to more than 0.15 in the Gironde
311 Estuary at Pauillac. Shapes of the spectra are also very variable. The mark of strong chlorophyll-a absorption
312 around 670 nm is well observed in the Chascomús and Spuikom lakes as well as in some spectra of the Belgian
313 coastal waters. The two extremely turbid sampling stations, the Rio de la Plata and the Gironde at Pauillac, show
314 some similarities in their spectral shapes although a large variability is observed at Pauillac due to a larger impact
315 of tides.

316 The relationship of water reflectance at 645 and 860 nm and turbidity (Figure 9) shows expected patterns with a
317 saturation of the reflectance at 645 nm when turbidity is higher than 200 FNU- (Luo et al., 2018). Indeed, for these
318 extreme turbidity values the band at 860 nm shows a more linear relationship. ~~These results also show the limits~~
319 ~~of the standard algorithm of Neehad et al. (2009) for high turbidity or in case of a different environment like the~~
320 ~~Chaseomús lake which is characterized by high [Chl a] and turbidity.~~

a mis en forme : Couleur de police : Rouge, Barré

321 5. Conclusion

322 Coastal and inland waters strongly interact with human activities. Some of these activities, like fisheries or tourism,
323 rely on a good ecological status whereas the same activities but also others like farming, industry or urbanization
324 tend to affect water quality. Hence, monitoring these waters is extremely important and for that optical remote
325 sensing is a valuable tool as it allows a large spatial and temporal coverage. However, it is still challenging to
326 retrieve biogeochemical parameters in complex case 2 waters (Odermatt et al., 2012) because the transfer of light
327 in water is affected by temporally and spatially variable inputs of CDOM and terrestrial sediments. To help the
328 scientific community to build comprehensive database for the development of algorithms, the HYPERMAQ da-
329 taset provides data for sevensix different studies areas with SPM and [Chl-a] ranging from moderate to extremely
330 turbid and productive, and located over three continents (i.e. Europe, South America and Asia). The HYPERMAQ
331 dataset includes big river estuaries characterized by high turbidity, inland lagoons with productivity ranging from
332 moderate to extreme and finally Belgian coastal waters in the North Sea characterized by the high spatio-temporal
333 variability of optical properties (Vantrepotte et al., 2012). The parameters shared in the HYPERMAQ dataset
334 include descriptors of biogeochemical conditions (i.e. [Chl-a], SPM, turbidity) as well as AOPs (i.e. water reflec-
335 tance) and IOPs (a_{nw} and c_{nw}). Although this dataset does not aim to cover the whole variability of case 2 waters,
336 it provides valuable information to describe turbid and even extremely turbid waters and has the potential to help
337 the development of remote sensing algorithms. It can also contribute to the production of a larger optical database,
338 based on in situ measurements for a comprehensive description of case 2 waters.

339

340 Data availability

341 Data is available from Lavigne et al. (2022), hosted at PANGAEA (<http://www.pangaea.de>) under the doi:
342 <https://doi.pangaea.de/10.1594/PANGAEA.944313>. The HYPERMAQ dataset is subdivided into 10 sub-datasets
343 with their own DOI: absorptions and attenuation data (<https://doi.pangaea.de/10.1594/PANGAEA.944361>), Chl-
344 a concentration, turbidity and organic and inorganic sediments concentrations (<https://doi.pangaea.de/10.1594/PANGAEA.944364>), pigment concentrations (<https://doi.pangaea.de/10.1594/PANGAEA.944321>), spectral downwelling irradiance (<https://doi.pangaea.de/10.1594/PANGAEA.944311>) and its
345 standard deviation (<https://doi.pangaea.de/10.1594/PANGAEA.944312>), downwellingsky radiance
346 (<https://doi.pangaea.de/10.1594/PANGAEA.944380>) and its standard deviation (<https://doi.pangaea.de/10.1594/PANGAEA.944385>), water downwelling radiance (<https://doi.pangaea.de/10.1594/PANGAEA.944369>) and its standard deviation (<https://doi.pangaea.de/10.1594/PANGAEA.944371>) and finally water
347 reflectance (<https://doi.pangaea.de/10.1594/PANGAEA.944474>) and its standard deviation (<https://doi.pangaea.de/10.1594/PANGAEA.944475>).

a mis en forme : Couleur de police : Automatique

a mis en forme : Couleur de police : Automatique

a mis en forme : Couleur de police : Automatique

353 **Author contributions**

354 HL, AD, DD, [FCFS](#), AC, XS, JIG, RP, MB, QV and KR participated to one or more field campaigns. Data pro-
355 cessing has been made by HL, AD and JIG (turbidity), DD (absorption), KR, MB, QV, RP, AD (water reflectance),
356 AC, AD, DD, [FCFS](#), KS (chlorophyll-a, pigments and SPM). HL, DD, AD have compiled data and created the
357 final dataset. All authors participated to manuscript redaction and revision.

358 **Competing interests.**

359 The authors declare that they have no conflict of interest.

360 **Acknowledgements**

361 This work has been founded and promoted by the Research programme for earth observation 580 STEREO III
362 HYPERMAQ project (contract nr SR/00/335). Flemish LifeWatch BE programme, funding by FWO, is thanks for
363 its contribution to the water sampling in the Belgian Coastal Zone. We thank VLIZ for providing the Zeekat and
364 shiptime on the RV Simon Stevin and her crew for their support during sampling. Inland water sampling in
365 Belgium was also founded by the Belspo PONDER (SR/00/325) project. The SAPIGH analytical platform of the
366 “Institut de la Mer de Villefranche” (CNRS-France) is thanks for having performed the analysis of pigments in the
367 Gironde. NASA, USGS, ESA and EUMETSAT are thanks to offer a free access to Landsat 8 and Sentinel 2
368 images.

369 **References**

- 370 Abril, G., Etcheber, H., Le Hir, P., Bassoullet, P., Boutier, B., & Frankignoulle, M., Oxic/anoxic oscillations and
371 organic carbon mineralization in an estuarine maximum turbidity zone (The Gironde, France). *Limnology and*
372 *Oceanography*, 44 (5), 1304–1315, 1999.
- 373 Aubriot, L., Zabaleta, B., Bordet, F., Sienna, D., Risso, J., Achkar, M., & Somma, A., Assessing the origin of a
374 massive cyanobacterial bloom in the Río de la Plata (2019): Towards an early warning system. *Water Research*,
375 181, 115944, 2020.
- 376 Castaing, P., & Allen, G.P., Mechanisms of seaward escape of suspended sediment from the Gironde: a macrotidal
377 estuary in France. *Marine Geology* 40, 101–118, 1981.
- 378 Castagna, A., Amadei Martínez, L., Bogorad, M., Daveloose, I., Dasseville, R., Dierssen, H. M., Beck, M., Mor-
379 telmans, J., Lavigne, H., Dogliotti, A., Doxaran, D., Ruddick, K., Vyverman, W., & Sabbe, K., Optical and bioge-
380 ochemical properties of Belgian inland and coastal waters, *Earth Syst. Sci. Data Discuss.*
381 <https://doi.org/10.5194/essd-2021-466>, in press, 2022.
- 382 Chen, Z., Saito, Y., Hori, K., Zhao, Y., & Kitamura, A., Early Holocene mud-ridge formation in the Yangtze
383 offshore, China: a tidal-controlled estuarine pattern and sea-level implications. *Marine Geology*, 198(3-4), 245-
384 257, 2003.

385 Diovisalvi, N., Berasain, G., Unrein, F., Colautti, D., Fermani, P., Llames, M.E., Torremorel, A.M., Lagomarsino,
386 L., Pérez, G., Escaray, R., Bustingorry, J., Ferraro, M. & Zagarese, H., Chascomús: estructura y funcionamiento
387 de una laguna pampeana turbia. *Ecología Austral* 20, 115–127, 2010.

388 Diovisalvi, N., Salcedo Echeverry, G.E., Lagomarsino, L. & Zagarese, M.E., Seasonal patterns and responses
389 to an extreme climate event of rotifers community in a shallow eutrophic Pampean lake. *Hydrobiologia* 1 (1), 13,
390 2014.

391 Dogliotti, A. I., Camiolo, M., Simionato, C., Jaureguizar, A. J., Guerrero, R. A., & Lasta, C. Á., First optical
392 observations in the turbidity maximum zone in the Río de la Plata estuary: A challenge for atmospheric correction
393 algorithms. *Ocean Optics XXII (USA, 26 al 31 de octubre de 2014)*, 2014.

394 Dogliotti, A. I., Ruddick, K., & Guerrero, R., Seasonal and inter-annual turbidity variability in the Río de la Plata
395 from 15 years of MODIS: El Niño dilution effect. *Estuarine, Coastal and Shelf Science*, 182, 27-39, 2016.

396 Dogliotti, A. I., Gossn, J. I., Gonzalez, C., Yema, L., Sanchez, M., & O'Farrell, I. L., Evaluation of Multi-and
397 Hyper-Spectral Chl-A Algorithms in the Río De La Plata Turbid Waters During a Cyanobacteria Bloom. In 2021
398 IEEE International Geoscience and Remote Sensing Symposium IGARSS (pp. 7442-7445). IEEE, 2021.

399 Doxaran, D., Froidefond, J.M., Lavender, S.J. & Castaing P., Spectral signature of highly turbid waters. Applica-
400 tion with SPOT data to quantify suspended particulate matter concentrations. *Remote Sensing of Environment*,
401 81, 149-161, 2002.

402 Doxaran D., Babin M. & Leymarie, E., Near-infrared light scattering by particles in coastal waters. *Optics Express*,
403 15(20), 12834-12849, 2007.

404 Doxaran, D., Froidefond, J.M., Castaing, P. & Babin, M., Dynamics of the turbidity maximum zone in a ma-
405 crotidal estuary (the Gironde, France): Observations from field and MODIS satellite data. *Estuarine, Coastal and*
406 *Shelf Science* 81, 321–332, 2009a.

407 Doxaran, D., Ruddick, K., McKee, D., Gentili, B., Tailliez, D., Chami, M., Babin, M., Spectral variations of light
408 scattering by marine particles in coastal waters, from the visible to the near infrared. *Limnology and Oceanogra-*
409 *phy*, 54, 1257-1271, 2009b.

410 Flanders Marine Institute. (2021). -LifeWatch observatory data: nutrient, pigment, suspended matter and secchi
411 measurements in the Belgian Part of the North Sea, <https://doi.org/10.14284/441>, 2021.

412 Framiñan, M. B., & Brown, O.B., Study of the Río de la Plata turbidity front: I. Spatial and temporal distribu-
413 tion. *Continental Shelf Research*, 16, 1259-1282.-1996.

414 Hieronimi, M., Krasemann, H., Müller, D., Brockmann, C., Ruescas, A., Stelzer, K., ... & Regner, P. (2016). *Ocean*
415 *colour remote sensing of extreme case-2 waters. spectrum, 2, 4.*

416 Hieronimi, M., Müller, D., & Doerffer, R. (2017). *The OLCI Neural Network Swarm (ONNS): a bio-geo-optical*
417 *algorithm for open ocean and coastal waters. Frontiers in Marine Science, 4, 140.*

418 Irigoien, X., & Castel, J., Light limitation and distribution of chlorophyll pigments in a highly turbid estuary: the
419 Gironde (SW France). *Estuarine, Coastal and Shelf Science*, 44, 507– 517, 1997.

420 Jespersen, A.M. & Christoffersen, K., Measurements of chlorophyll-a from phytoplankton using ethanol as ex-
421 traction solvent. *Archiv für Hydrobiologie* 109: 445-454, 1987.

a mis en forme : Anglais (États-Unis)

a mis en forme : Anglais (Royaume-Uni)

a mis en forme : Anglais (Royaume-Uni)

a mis en forme : Anglais (Royaume-Uni)

a mis en forme : Anglais (Royaume-Uni)

422 Lacroix, G., Ruddick, K., Ozer, J., & Lancelot, C., Modelling the impact of the Scheldt and Rhine/Meuse plumes
423 on the salinity distribution in Belgian waters (southern North Sea). *Journal of Sea Research*, 52(3), 149-163, 2004.

424 Lancelot, C., Spitz, Y., Gypens, N., Ruddick, K., Becquevort, S., Rousseau, V., Lacroix, G. & Billen, G., Model-
425 ling diatom and Phaeocystis blooms and nutrient cycles in the Southern Bight of the North Sea: the MIRO model.
426 *Marine Ecology Progress Series*, 289, 63-78, 2005.

427 Lavigne, H., Dogliotti, A., Doxaran, D., Shen, F., Castagna, A., Beck, B., Vanhellefont, Q., Sun, X., Gossn, J.
428 I.; Pannipullath, R., Sabbe, K., Vansteenwegen, D., Ruddick, K., The HYPERMAQ dataset. PANGAEA,
429 <https://doi.pangaea.de/10.1594/PANGAEA.944313>. 2022

430 Li, P., Yang, S. L., Milliman, J. D., Xu, K. H., Qin, W. H., Wu, C. S., Y. P. Chen, & Shi, B. W., Spatial, temporal,
431 and human-induced variations in suspended sediment concentration in the surface waters of the Yangtze Estuary
432 and adjacent coastal areas. *Estuaries and Coasts*, 35(5), 1316-1327. 2012.

433 Luo, W., Shen, F., He, Q., Cao, F., Zhao, H., & Li, M., Changes in suspended sediments in the Yangtze River
434 Estuary from 1984 to 2020: Responses to basin and estuarine engineering constructions. *Science of The Total*
435 *Environment*, 805, 150381, 2022.

436 Mackey, M. D., Mackey, D. J., Higgins, H. W., & Wright, S. W., CHEMTAX-a program for estimating class
437 abundances from chemical markers: application to HPLC measurements of phytoplankton. *Marine Ecology Pro-*
438 *gress Series*, 144, 265-283, 1996.

439 Morel, A., & Maritorena, S., Bio-optical properties of oceanic waters: A reappraisal. *Journal of Geophysical Re-*
440 *search: Oceans*, 106(C4), 7163-7180, 2001.

441 Morel, A., & Prieur, L., Analysis of variations in ocean color 1. *Limnology and oceanography*, 22(4), 709-722,
442 1977.

443 Mortelmans, J., Deneudt, K., Cattrijsse, A., Beauchard, O., Daveloose, I., Vyverman, W., Vanaverbeke, J., Tim-
444 mermans, K., Peene, J., Roose, P., Knockaert, M., Chou, L., Sanders, R., Stinchcombe, M., Kimpe, P., Lammens,
445 S., Theetaert, H., Gkritzalis, T., Hernandez, F., and Mees, J.: Nutrient, pigment, suspended matter and turbidity
446 measurements in the Belgian part of the North Sea, *Scientific Data*, 22, [https://doi.org/10.1038/s41597-019-0032-](https://doi.org/10.1038/s41597-019-0032-7)
447 [7](https://doi.org/10.1038/s41597-019-0032-7), 2019.

448 Muylaert, K., Gonzales, R., Franck, M., Lionard, M., Van der Zee, C., Cattrijsse, A., Sabbe, K., Chou, L. & Vyver-
449 man, W., Spatial variation in phytoplankton dynamics in the Belgian coastal zone of the North Sea studied by
450 microscopy, HPLC-CHEMTAX and underway fluorescence recordings. *Journal of Sea Research*, 55(4), 253-265,
451 2006.

452 ~~Nechad, B., Ruddick, K. G., & Neukermans, G., Calibration and validation of a generic multisensor algorithm for~~
453 ~~mapping of turbidity in coastal waters. In Remote Sensing of the Ocean, Sea Ice, and Large Water Regions 2009~~
454 ~~(Vol. 7473, p. 74730H). International Society for Optics and Photonics, 2009.~~

455 ~~Nechad, B., Dogliotti, A., Ruddick, K., & Doxaran, D., Particulate backscattering and suspended matter concen-~~
456 ~~tration retrieval from remote-sensed turbidity in various coastal and riverine turbid waters. In Proceedings of ESA~~
457 ~~living planet symposium, Prague (pp. 9-13), 2016.~~

458 Neukermans, G., Ruddick, K., Loisel, H., & Roose, P., Optimization and quality control of suspended particulate
459 matter concentration measurement using turbidity measurements. *Limnology and Oceanography: Methods*,
460 10(12), 1011-1023, 2012.

461 Odermatt, D., Gitelson, A., Brando, V. E., & Schaepman, M., Review of constituent retrieval in optically deep and
462 complex waters from satellite imagery. *Remote sensing of environment*, 118, 116-126, 2012.

463 Pérez, G.L., Llames, M.E., Lagomarsino, L., Zagarese, H., Seasonal variability of optical properties in a highly
464 turbid lake (Laguna Chascomús, Argentina). *Photochemistry and Photobiology*, 87: 659–670, 2011.

465 Ruddick, K. G., Cauwer, V. D., Park, Y. J., and Moore, G., Seaborne measurements of near infrared water-leaving
466 reflectance: The similarity spectrum for turbid waters, *Limnol. Oceanogr.*, 51, 1167–1179, 2006.

467 Shen, F., Verhoef, W., Zhou, Y., Salama, M., & Liu, X., Satellite estimates of wide-range suspended sediment
468 concentrations in Changjiang (Yangtze) estuary using MERIS data. *Estuaries and Coasts*, 33(6), 1420-1429, 2010a

469 Shen, F., Zhou, Y. X., Li, D. J., Zhu, W. J., & Suhyb Salama, M., Medium resolution imaging spectrometer
470 (MERIS) estimation of chlorophyll-a concentration in the turbid sediment-laden waters of the Changjiang (Yang-
471 tze) Estuary. *International Journal of Remote Sensing*, 31(17-18), 4635-4650, 2010b.

472 Shen, F., Zhou, Y., Li, J., He, Q., & Verhoef, W., Remotely sensed variability of the suspended sediment concen-
473 tration and its response to decreased river discharge in the Yangtze estuary and adjacent coast. *Continental Shelf*
474 *Research*, 69, 52-61, 2013.

475 Shen, F., Tang, R., Sun, X., & Liu, D., Simple methods for satellite identification of algal blooms and species
476 using 10-year time series data from the East China Sea. *Remote Sensing of Environment*, 235, 111484, 2019.

477 Tilstone, G. H., Moore, G. F., Sørensen, K., Doerffer, R., & Røttgers, R., REVAMP Protocols. REVAMP metho-
478 dologies – EVG1 – CT – 2001 – 00049. http://envisat.esa.int/workshops/mavt_2003/MAVT-2003_802_RE-
479 [VAMPprotocols3.pdf](http://envisat.esa.int/workshops/mavt_2003/MAVT-2003_802_RE-VAMPprotocols3.pdf), 2002.

480 Torremorell, A., J. Bustigorry, R. Escaray & Zagarese, H. E., Seasonal dynamics of a large, shallow lake, laguna
481 Chascomús: the role of light limitation and other physical variables. *Limnologica* 37: 100–108, 2007.

482 Torremorell, A., M. E. Llames, G. L. Pérez, R. Escaray, J. Bustigorry & Zagarese, H. E., Annual patterns of
483 phytoplankton density and primary production in a large, shallow lake: the central role of light. *Freshwater Biology*
484 54: 437–449, 2009.

485 Uitz, J., Claustre, H., Morel, A., & Hooker, S. B. Vertical distribution of phytoplankton communities in open
486 ocean: An assessment based on surface chlorophyll. *Journal of Geophysical Research: Oceans*, 111(C8), 2006.

487 Van der Linde, D. W., Protocol for the determination of total suspended matter in oceans and coastal zones. Joint
488 Research Centre, Ispra. Technical note I.98.182, 1998.

489 Van Heukelem, L., & Thomas, C. S., Computer-assisted high-performance liquid chromatography method devel-
490 opment with applications to the isolation and analysis of phytoplankton pigments. *Journal of Chromatography A*,
491 910(1), 31-49, 2001.

492 Vantrepotte, V., Loisel, H., Dessailly, D., & Mériaux, X., Optical classification of contrasted coastal waters. *Re-*
493 *mote Sensing of Environment*, 123, 306-323, 2012.

a mis en forme : Français (France)

a mis en forme : Français (France)

Code de champ modifié

a mis en forme : Français (France)

a mis en forme : Français (France)

a mis en forme : Anglais (Royaume-Uni)

a mis en forme : Anglais (Royaume-Uni)

494 Zhu, W., Wang, M., & Zhang, B., The effects of urbanization on PM2. 5 concentrations in China's Yangtze River
495 Economic Belt: New evidence from spatial econometric analysis. *Journal of cleaner production*, 239, 118065,
496 2019.

497 **Table 1: Date, location and platform of the campaigns.**
 498

| Campaign | Date | Platform | Latitude (deg) | Longitude (deg) |
|--------------------------------------|---------------------------------------|-----------------|----------------|-----------------|
| Spuikom | 19 April 2018, 23,24 and 27 July 2018 | Inflatable boat | 51.23 | 2.95 |
| Belgian Coastal waters | 23-25 April 2018, 25-26 July 2018 | RV Simon Stevin | 51.18-51.59 | 2.50-3.15 |
| Gironde (Pauillac) | 17 and 19 Sept. 2018 | Harbor | 45.1975 | -0.7422 |
| Gironde (Le Verdon) | 18 and 20 Sept. 2018 | Pier | 45.5438 | -1.042 |
| Chascomús | 9-10 April 2018 | Pier | -35.5828 | -58.0202 |
| Rio de la Plata (Buenos Aires) | 4-5 April 2018 | Pier | -34.5609 | -58.3988 |
| Xangtze Yangtze (Chongxi) | 31 May, 1 and 3 June 2018 | Pier | 31.759 | 121.193 |
| Xangtze Yangtze (Baozhen) | 4-8 June 2018 | Pier | 31.520 | 121.609 |

499 **Table 2: Number of observations for each sampling site. *also include pigments concentrations from HPLC.**
 500

| Campaign / Site | TriOS | TUR (HACH) | TUR (OBS) | $a_{440} - C_{440}$ AC-9 | SPM | [Chl-a] |
|--------------------------------------|-------|------------|-----------|--------------------------|------|---------|
| Spuikom | 27 | 27 | 23 | 11 | 17 | 17* |
| Belgian coastal waters | 18 | 19 | 17 | 10 | 19 | 18* |
| Gironde - Pauillac | 25 | 26 | 26 | 23 | 13 | 13* |
| Gironde - Le Verdon | 21 | 25 | 25 | 24 | 12 | 12* |
| Chascomús | 5 | 5 | 5 | 5 | 5 | 3 |
| Rio de la Plata- BA | 16 | 22 | 22 | 18 | 10 | 10 |
| Xangtze Yangtze - Chongxi | - | 1916 | - | - | 1716 | - |
| Xangtze Yangtze - Baozhen | - | 37 | - | 29 | 37 | - |

501
 502
 503 **Table 3: Distribution of SPM (g m⁻³) in each sampling site.**

| Campaign / Site | SPM (g m ⁻³) | | | |
|--------------------------------------|--------------------------|--------|------|-------|
| | min | median | mean | max |
| Spuikom | 2.06 | 3.16 | 3.93 | 8.40 |
| Belgian coastal waters | 1.02 | 4.49 | 9.63 | 62.04 |
| Gironde - Pauillac | 22.5 | 181 | 177 | 474 |
| Gironde - Le Verdon | 5.85 | 7.80 | 10.2 | 23.5 |
| Chascomús | 81.0 | 175 | 141 | 189 |
| Rio de la Plata | 49.3 | 71.7 | 74.0 | 93.8 |
| Xangtze Yangtze - Chongxi | 27.2 | 42.2 | 44.8 | 66.4 |
| Xangtze Yangtze - Baozhen | 23.6 | 52.8 | 53.6 | 138.4 |

504
 505
 506

507 **Table 4: Distribution of Chl-a concentration (mg m⁻³) in each sampling site.**

508

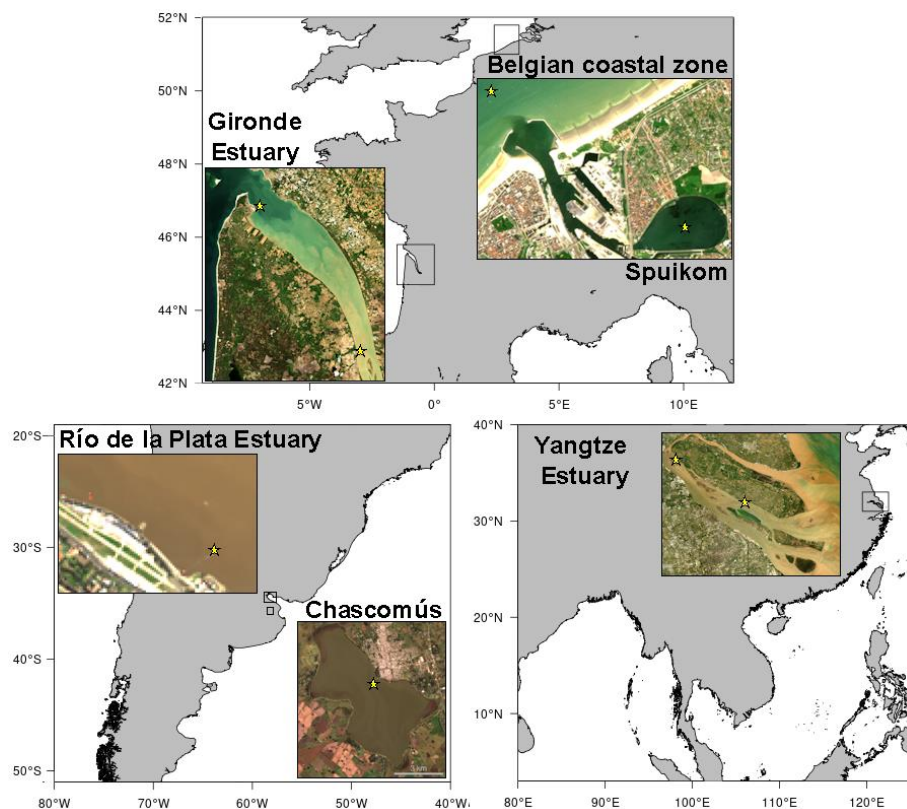
| Campaign / Site | Chl-a (mg m ⁻³) | | | |
|-------------------------------------|-----------------------------|--------|-------|-------|
| | min | median | mean | max |
| Spuikom | 2.40 | 9.16 | 10.64 | 22.70 |
| Belgian coastal waters | 1.99 | 6.33 | 7.49 | 17.36 |
| Gironde - Pauillac | 2.49 | 3.82 | 3.88 | 6.85 |
| Gironde – Le Verdon | 0.91 | 1.63 | 1.67 | 2.79 |
| Chascomús | 141.5 | 141.5 | 154.6 | 180.7 |
| Rio de la Plata-BA | 2.17 | 3.27 | 3.72 | 8.71 |
| XangtzeYangtze - Chongxi | - | - | - | - |
| XangtzeYangtze - Baozhen | - | - | - | - |

509

510

511

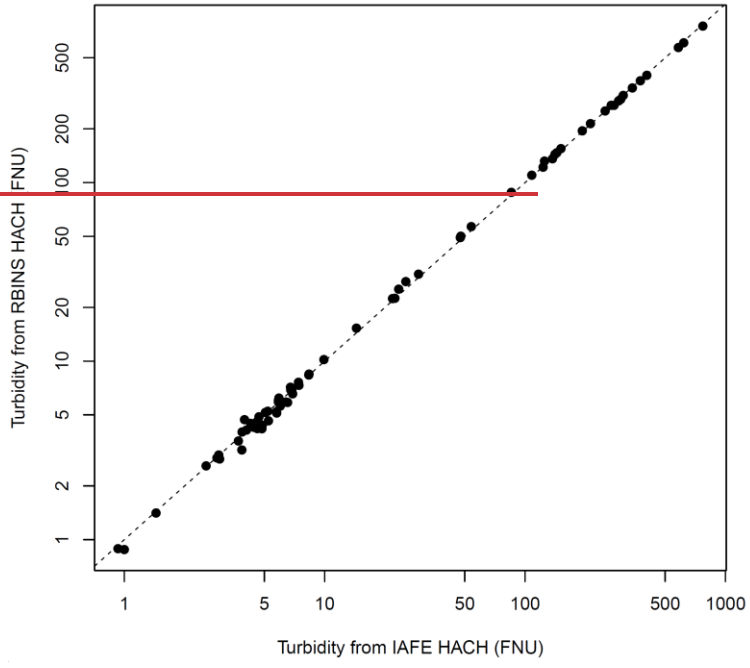
512
513



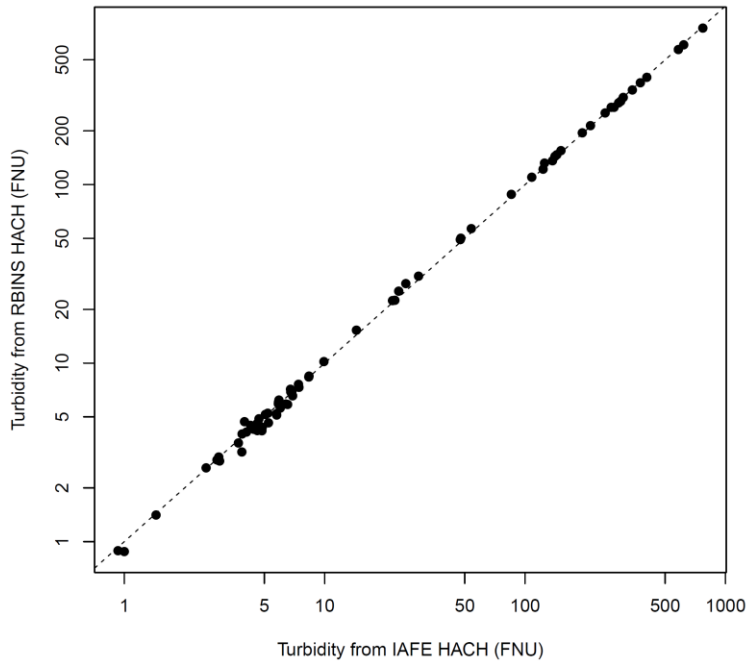
514
515 **Figure 1:** Locations of the study areas. Satellite images are coming from Landsat 8 OLI (Yangtze: image taken on 2021-
516 04-29, ~~Chascomús~~Chascomús: image taken on 10-05-2017, Río de la Plata: image taken on 2014-08-13) and Sentinel 2B
517 MSI (Belgian Coastal Zone: image taken on 2021-05-30, Gironde: image taken on 2021-05-03)

518
519
520

a mis en forme : Espagnol (Espagne)



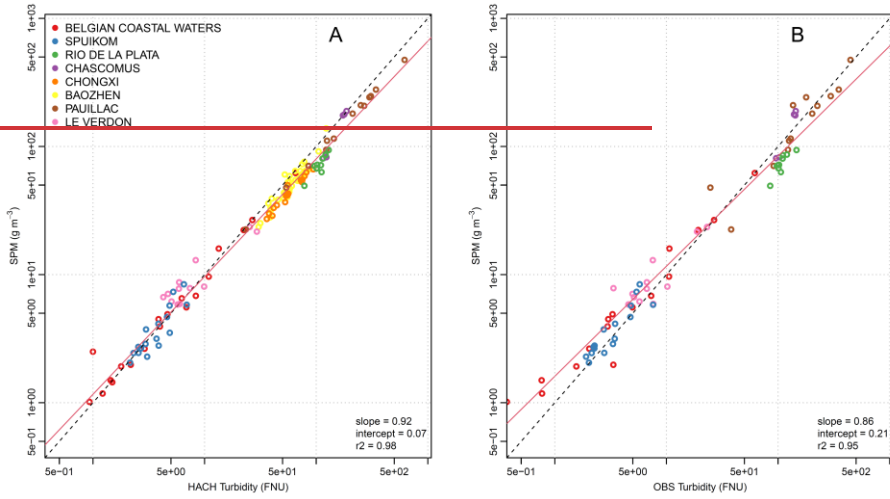
521



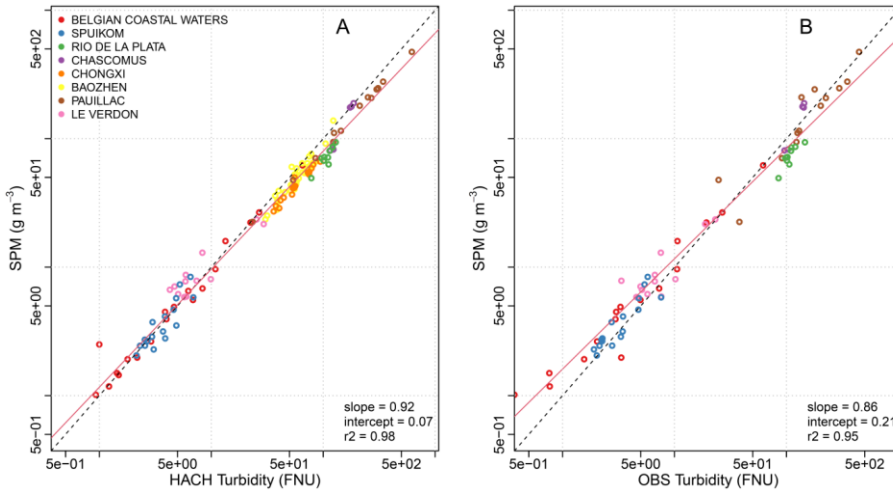
522
523 **Figure 2: Comparison of simultaneous measurements of turbidity made from two different HACH instruments**
524 **($r^2=0.99$).**

525

526



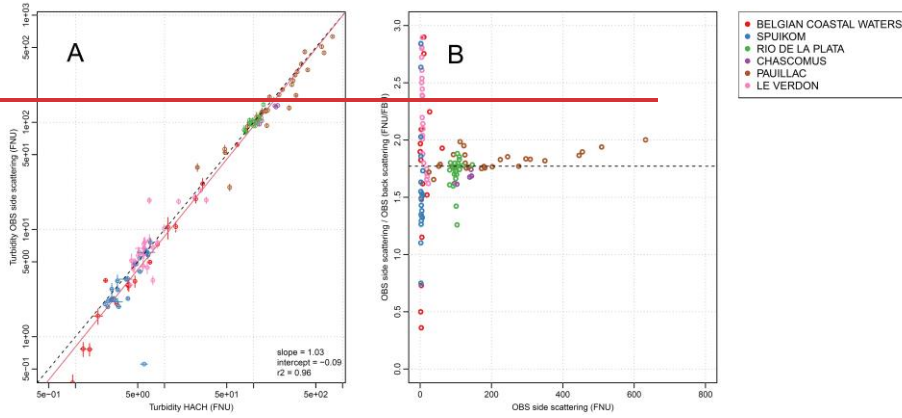
527



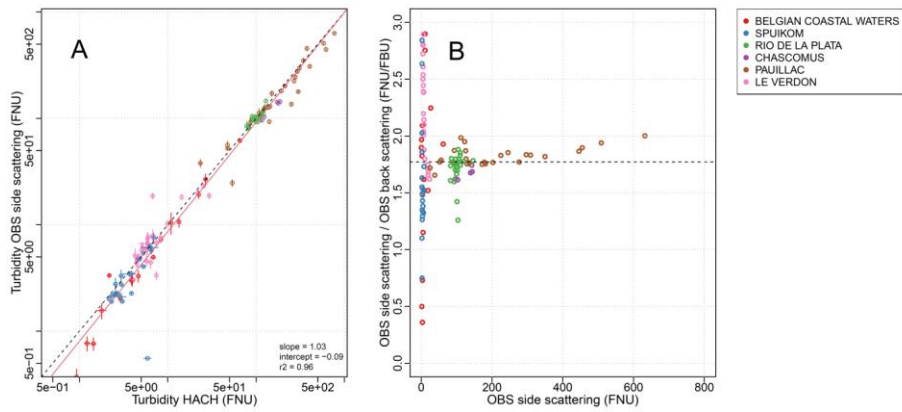
528

529 **Figure 3: SPM as a function of turbidity. Turbidity from OBS is given by the side-scattering measurement. The dotted**
530 **line is the 1:1 line and the red line represents the linear regression between SPM and turbidity.**

531



532

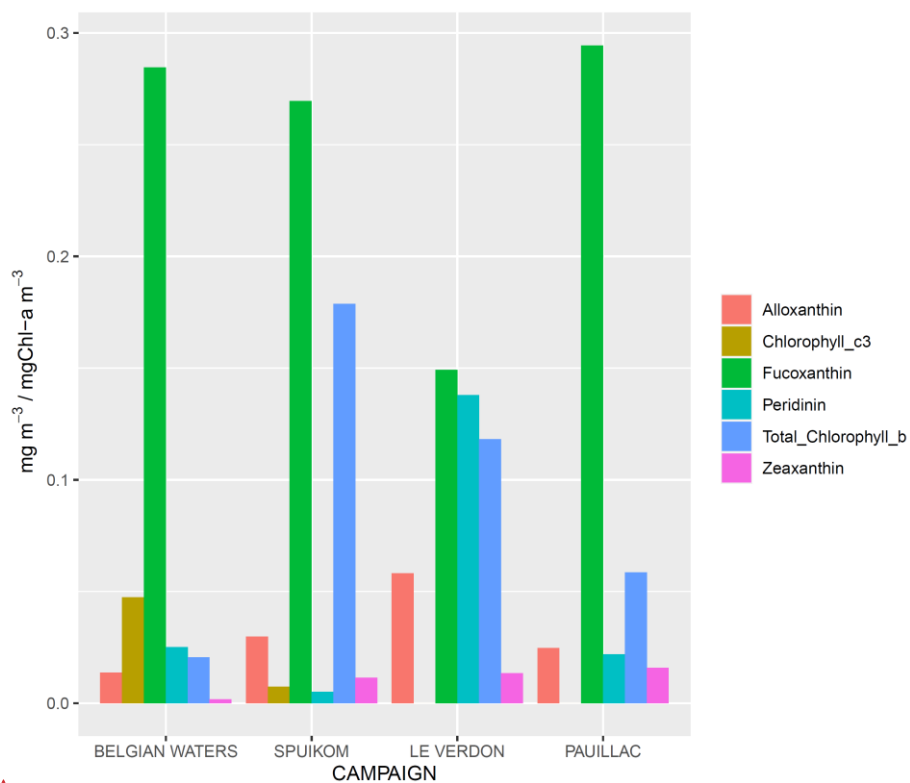


533

534 **Figure 4: Turbidity measured by HACH instrument as a function of side-scattering turbidity measured by the OBS**
 535 **instrument (panel A). The red line shows the least squares regression between these variables. Panel B: ratio of the OBS**
 536 **side-scattering to backscattering ratio as a function of the OBS side-scattering. The horizontal dotted line represents**
 537 **the median value of the scattering ratio.**

538

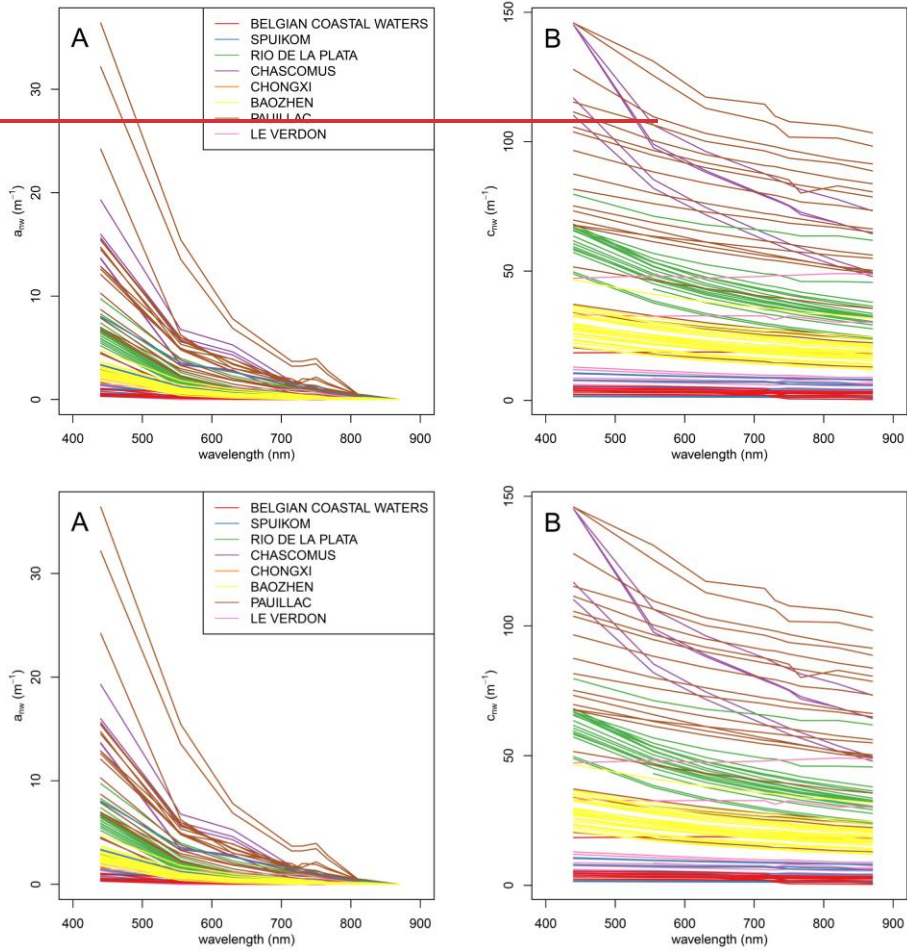
539



a mis en forme : Espagnol (Espagne)

540
 541 **Figure 5: For each campaign, average concentration of alloxanthin, fucoxanthin, peridinin, chlorophyll c3, zeaxanthin**
 542 **and total chlorophyll b normalized by the concentration in chlorophyll-a**

543



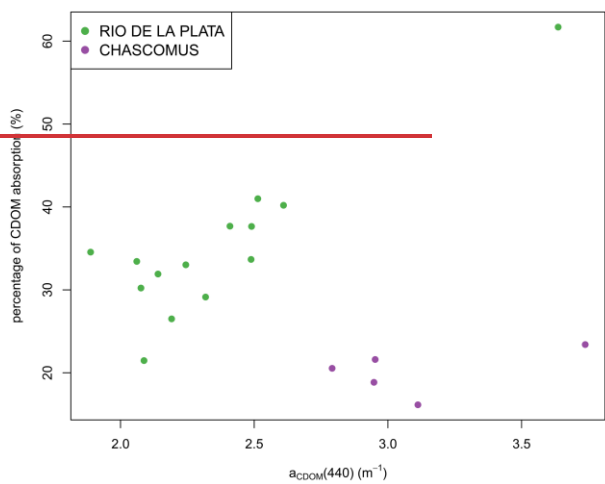
544

545

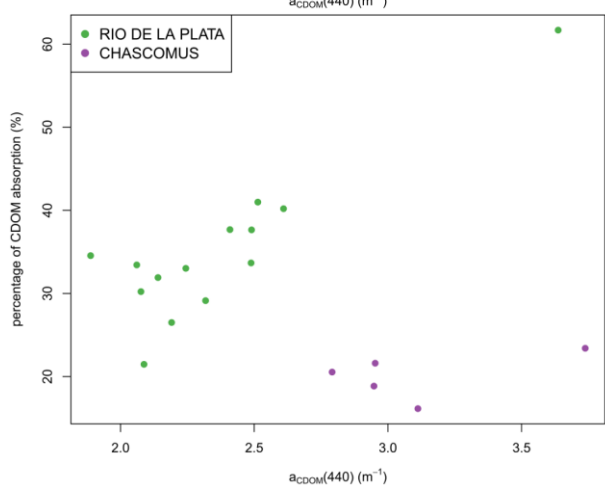
546 **Figure 6: Non-water absorption (panel A) and attenuation coefficients (panel B) measured with the ACtheAC-9 instru-**
 547 **ment.**

548

549



550

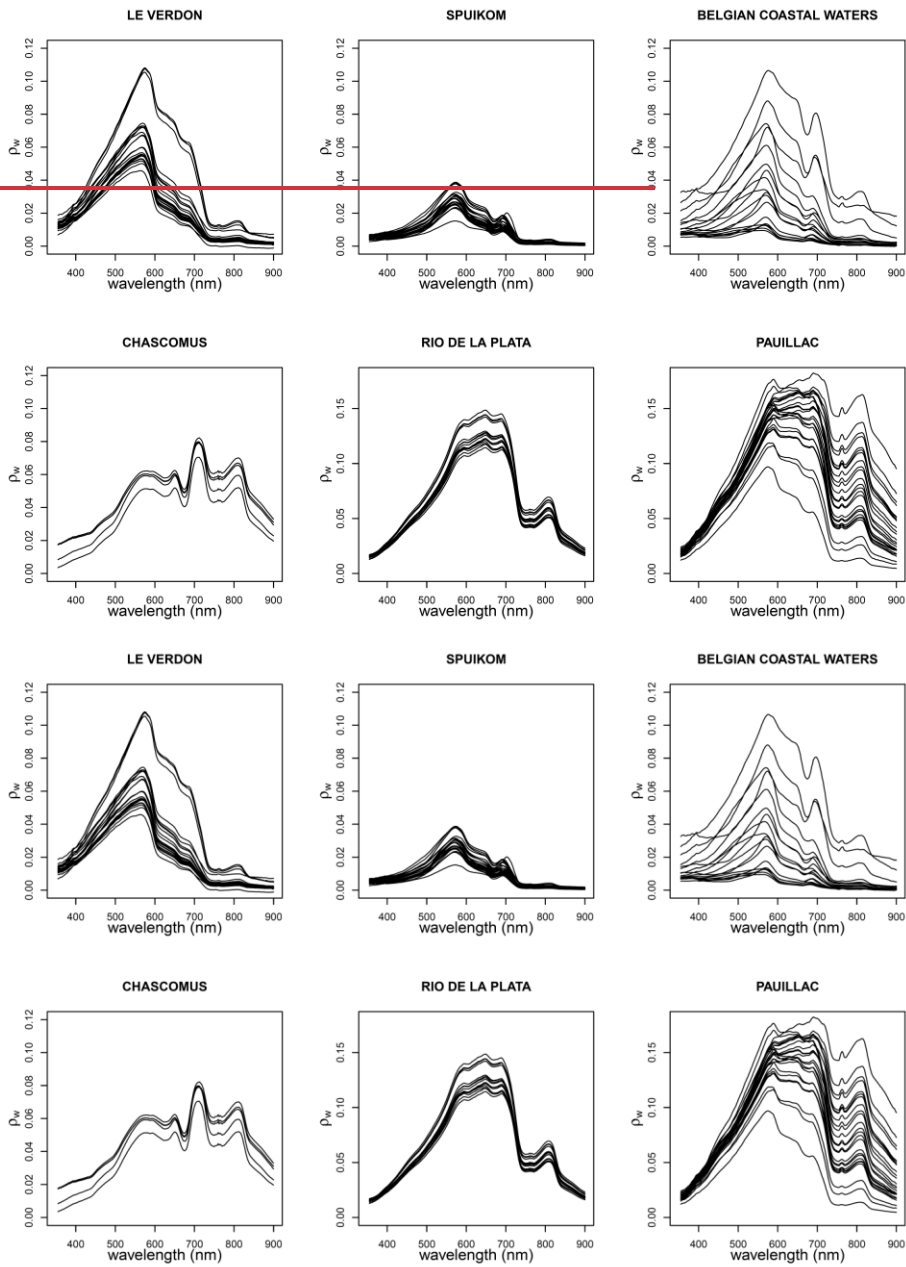


551

552

553

Figure 7: Percentage of CDOM absorption as a function of $a_{CDOM}(440)$. a_{CDOM} was only measured during two campaigns.

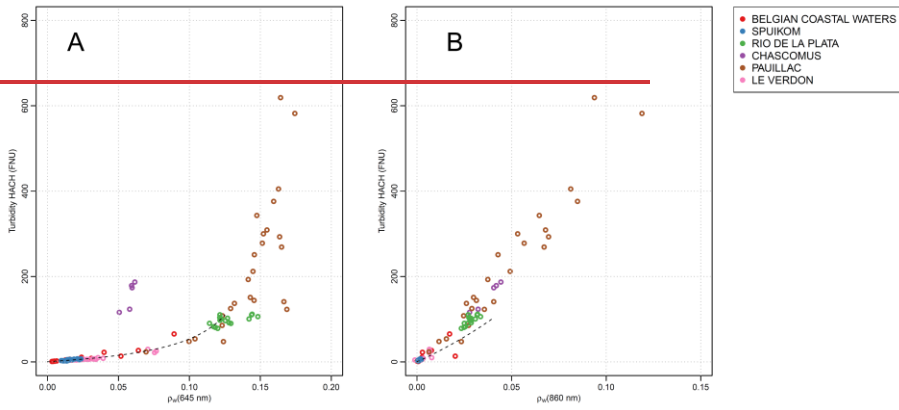


554

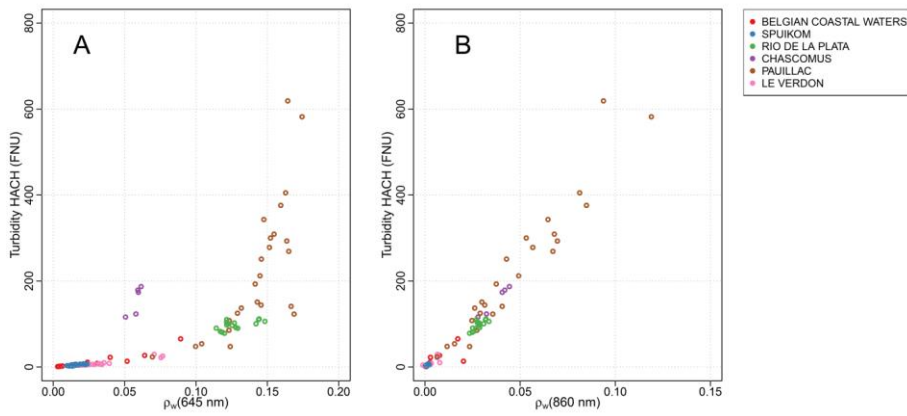
555

556 **Figure 8: Water reflectance spectra (unitless) from each sample site.**

557
558



559



560

561 **Figure 9: Turbidity as a function of water reflectance at 645 nm (panel A) and 850 nm (panel B). Black dotted line**
562 **represents the model of Nechad et al. (2009) between 0 and 100 FNU.**